DESKTOP USE OF COMPUTATIONAL FLUID DYNAMICS TO DESIGN AND TROUBLESHOOT COMPRESSORS AND TURBOEXPANDERS

by

Grant Nordwall

Senior Machinery Engineer

Jigger Jumonville

Senior Consulting Engineer

Mafi-Trench Corporation

Santa Maria, California

and

Terryl Matthews

Principal Rotating Equipment Specialist

Bechtel Corporation

Houston, Texas

Grant Nordwall is a Senior Machinery Engineer for Mafi-Trench Corporation, in Santa Maria, California. He has been with Mafi-Trench since 1990 working in the areas of machine design, performance testing, rotordynamic analysis, and aerodynamics including computational fluid dynamics.

Mr. Nordwall received his B.S. degree (Mechanical Engineering, 1990) from California Polytechnic State University. He has continued his education with rotordynamic and aerodynamic courses at Concepts NREC, Engineering Dynamics Inc., Rotordynamics Seal Research (RSR), AEA Technology, and Numeca. Mr. Nordwall is a registered Professional Engineer in the State of California.

Jigger Jumonville is a Senior Consulting Engineer for Mafi-Trench Corporation, in Santa Maria, California. He has been with them since 1990 and has held many titles including Chief Engineer. Mr. Jumonville is currently involved in mechanical, aerodynamic, and magnetic bearing product improvements, as well as troubleshooting unusual field problems. Previously, he worked for 10 years at the Dow Chemical Company in Plaquemine, Louisiana. Five of those years were spent as the Rotating Equipment Engineer in a world scale ethylene plant.

Mr. Jumonville received his B.S. degree (Mechanical Engineering, 1979) from Louisiana State University. While in school, he was a member of various honorary societies, including Pi Tau Sigma and Tau Beta Pi. He is a part-time professor at Cal Poly in San Luis Obispo, where he teaches a senior level Mechanical Engineering course in turbomachinery. Mr. Jumonville is a registered Professional Engineer in the State of Louisiana.

Terryl Matthews is a Principal Rotating Equipment Specialist with Bechtel Corporation, in Houston, Texas. He retired in 2003 from Dow Chemical, Design and Construction, after 30 years. His responsibilities there included specifications, technical support, mechanical and performance testing, consulting, and field assistance in the area of rotating equipment.

Mr. Matthews holds a B.S. degree (Mechanical Engineering, 1972) from the University of Houston. Author of six technical papers, he is a member of ASME, the Ethylene Producers Conference Rotating Machinery Subcommittee, and the ASME International Gas Turbine Institute's Industrial and Cogeneration Committee. He is a former member of the API Committee on Refinery Equipment and sponsor for SOME, served on API Task Forces 613 and 677, is a former member of ASME B73 Committee, and is a registered Professional Engineer in the State of Texas.

ABSTRACT

For several decades, turboexpander designers have relied on experience and traditional design tools to create their products. Recent advances in CFD (computational fluid dynamics) software and desktop computing power have made it possible for some manufacturers to investigate unique fluid flow fields in routine design applications.

In this paper, four case studies of CFD in high performance expanders and compressors are discussed. The first case study shows CFD used as a screening tool for a radial inflow turbine stage. The second demonstrates a challenging compressor design, where CFD was integrated into the design process. The third case study details the uncommon application of CFD to a fluid film thrust bearing, showing comparisons to traditional bulk flow calculations. The fourth case study highlights the use of CFD in troubleshooting a centrifugal compressor stage. The CFD solution was subsequently verified by factory testing, and the equipment is successfully operating in the field.

INTRODUCTION

High speed turboexpanders are widely used in many industrial processes, including hydrocarbon processing, chemical, and air separation plants. The Seventh Edition of API 617 (2002) now includes a chapter on turboexpanders, which confirms their wide use and importance in our industry. The typical turboexpander includes a high speed, high efficiency turbine, direct coupled to either a centrifugal compressor or an electrical generator, with a rotor supported by either oil bearings or magnetic bearings.

The design tools discussed in this paper include FINE/Turbo by Numeca (CFD software), CCAD® by Concepts NREC (three-dimensional blade design and analysis software), NSFixed by Rotordynamics Seal Research (Navier-Stokes thrust bearing analysis), and various inhouse programs by Mafi-Trench Corporation.

While all four case studies relate to turboexpander components, the information and results can be applied to other machines that use centrifugal compressors or oil lubricated thrust bearings.

CASE 1—RADIAL INFLOW EXPANDER DESIGN

A turboexpander is used in hydrocarbon processing to refrigerate a gas stream, by removing work directly from the gas. By expanding the gas in a nearly isentropic fashion, energy in the high pressure gas entering the expander is removed and the gas exits at a lower pressure and temperature.

A radial inflow expander is able to accomplish near-isentropic expansion by a series of efficient energy conversions. The gas flows radially inward and is accelerated through inlet guide vanes and turned. The swirling, high velocity gas enters the expander impeller with relatively low incidence, because the blade tip velocity at the impeller outside diameter approximately matches the gas velocity. Work is extracted from the gas by removing this momentum: as the gas moves inward, it is forced to slow down because the blade tangential velocity decreases with the decreasing radius. The blades also turn the gas to reduce the gas velocity even further. As a result, the gas exits the impeller with low tangential velocity relative to the outside world. In this way, the angular momentum of the gas is efficiently removed. Up to 10 percent of the stage energy still remains as through-flow velocity at the impeller exit. Much of this remaining energy can be recovered with a conical diffuser. By converting the velocity into pressure, the static pressure at the turbine discharge is reduced, which results in additional refrigeration.

A radial inflow turbine is commonly designed for 50 percent reaction, with 50 percent of the enthalpy change occurring in the rotating section (the impeller). As an approximation, the "degree of reaction" is sometimes defined as the pressure drop across the rotor divided by the pressure drop across the stage.

As with most turbomachinery, the flow of gas through an expander stage encounters several rapid transitions. Although the guide vane and impeller geometry can be designed based on bulk flow assumptions, a CFD analysis provides insight into important localized fluid flow patterns, to refine the bulk-flow design.

The expander stage in this discussion incorporates an 8.5 inch (216 mm) diameter impeller, rotating at 26,000 rpm. It is designed to provide 50°F (30°C) of refrigeration from a 90 psi (6 bar) pressure drop, and will provide 860 hp (660 kW) of power to a centrifugal compressor mounted on the same shaft.

The CFD model for this stage included the inlet guide vanes, unshrouded rotor with tip clearance, and a conical diffuser. The computational mesh is shown in Figure 1. The CFD software's implementations of the k-epsilon turbulence model were used.

Inlet Guide Vanes

The pressure drop through the inlet guide vanes (IGVs) is used to accelerate the gas, as it turns toward a circumferential direction. The goal is to do this with a minimal loss in total pressure, with uniform velocity and flow angle at the IGV exit, and to create a minimal wake region downstream. A "nozzle efficiency" for the vanes can be defined as in Equation (1):

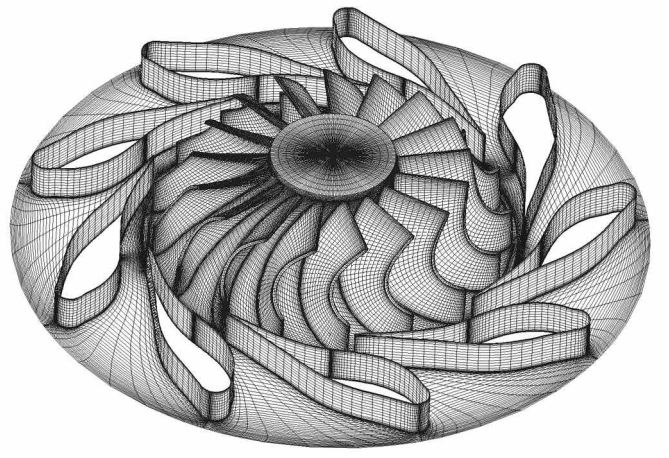

Figure 1. Radial Inflow Expander Computational Mesh.

$$Nozzle\ Efficiency = \frac{\left(h_{0T} - h_{1a}\right)}{\left(h_{0T} - h_{1ideal}\right)} \quad (1)$$

where:

h_{0T} = Total inlet enthalpy
h_{1a} = Actual IGV static exit enthalpy
h_{1ideal} = Ideal static outlet enthalpy

It should be noted that expansion through nozzles is an isenthalpic process, where the total enthalpy at the nozzle exit will be the same as the total enthalpy at the nozzle inlet (h_{0T}). The static enthalpies can be used when modeling the process as isentropic. However, there will be some loss of total pressure, as a portion of the inlet pressure is not converted to velocity, but increases the static temperature (heating caused by friction). This increase in static outlet temperature makes h_{1a} larger than h_{1ideal}, and thus results in an efficiency less than one.

The nozzle efficiency should be above 95 percent for well designed vanes.

Figure 2 and Figure 3 show the reduction in static pressure in the IGVs and the corresponding increase in velocity. The velocity and direction of the gas is relatively uniform at the exit of the IGV channel. The total pressure plot of Figure 4 indicates that the flow has accelerated with a minimal loss of total pressure. The plot also shows the wake regions, which are acceptably small. The resulting nozzle efficiency is 96 percent.

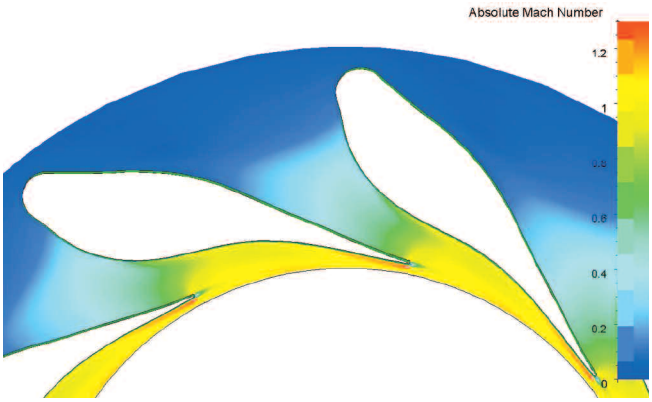

Figure 2. Absolute Mach Number Contour in Expander Inlet Guide Vanes.

Impeller

When an expander stage operates at 50 percent reaction, the tangential velocity at the IGV exit approximately matches the blade

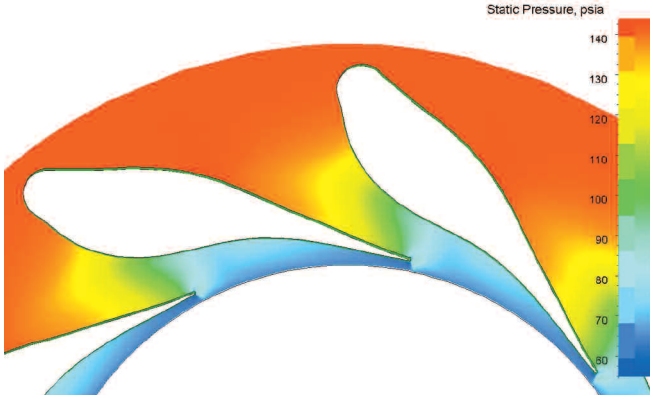

Figure 3. Static Pressure Contour in Expander Inlet Guide Vanes.

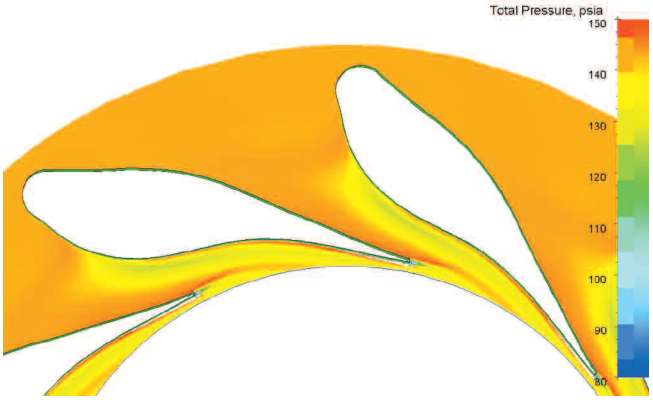

Figure 4. Total Pressure Contour in Expander Inlet Guide Vanes.

tip velocity. From a vantage point on the wheel, the flow appears to enter radially, and the blades are therefore radial at the inlet.

For expanders, the degree of reaction is often expressed in terms of a velocity ratio, or U_2/C_0. The change in enthalpy can be expressed in terms of velocity, with the velocity increase being proportional to the square root of the decrease in enthalpy across the entire stage. Thus the stage enthalpy drop is termed C_0, when expressed as velocity, as defined in Equation (2).

$$C_0 \propto \sqrt{dhs_{stage}} \tag{2}$$

where:
C_0 = Stage isentropic enthalpy change, expressed as velocity
dhs_{stage} = Stage isentropic enthalpy change, energy per unit mass

At 50 percent reaction, half the stage energy is converted to velocity through the IGVs, and the nozzle exit velocity will be as shown in Equation (3).

$$C_1 \propto \sqrt{0.5 * dhs_{stage}} \tag{3}$$

where:
C_1 = Velocity at nozzle exit
dhs_{stage} = Stage enthalpy drop

The C_1/C_0 will have a value of 0.707. The blade velocity at the wheel outside diameter is termed U_2, which is the product of diameter and speed. For zero incidence, the tangential component of C_1 should be matched to U_2. This will occur when U_2/C_0 is about 0.7.

For mechanical reasons, it is not always possible for the impeller to run fast enough to match the peripheral velocity exiting the IGVs. For this design, the U_2/C_0 value was limited to 0.49, and the reaction was only 20 percent. This leads to high incidence on the blades at the inlet and very little pressure drop available to accelerate the gas through the impeller.

The CFD analysis of the initial rotor design showed recirculation in the rotor passage, near the shroud (Figure 5). This is due to the high incidence. Separation also occurred at the trailing edge of the splitter blade, and this resulted in a substantial swirling of the gas entering the diffuser.

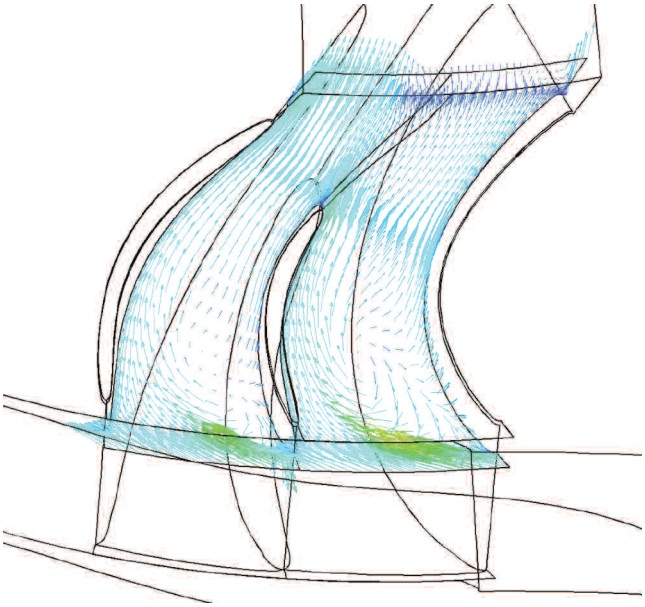

Figure 5. Relative Velocity Vectors near Shroud of Original Design.

To improve the flow in the rotor, the impeller blading was redesigned with the three-dimensional (3-D) blade design and analysis software and CFD to reduce incidence, give more control to the flow, and to prevent separation. This is challenging because the blade loading must remain high in order to turn the gas 95 degrees in just 3 inches (75 mm), at a velocity of 1000 ft/s (300 m/s), while also turning from radial to axial.

The 3-D flow visualization was instrumental in understanding this complex flowfield. The flow through the revised channel is shown in Figure 6, and the flow into the diffuser is shown in Figure 7. The final total-to-total rotor efficiency was 88.9 percent, which is respectable for a 0.49 U_2/C_0 application. With the modified rotor, the stage total-to-static efficiency increased from 80 percent to 83 percent.

Diffuser

The conical diffuser is an important element of a turboexpander stage, recovering the velocity exiting the impeller. In this example, the flow exiting the impeller is not uniform, it has a substantial amount of swirl, and is carrying over 10 percent of the stage energy in the form of velocity. The hub and shroud exit angles were modified to improve the diffuser recovery. The 3-D solution of the velocity field (Figure 8) shows a relatively uniform, decelerating flow. By interrogating the solution, the diffuser performance can be quantified in terms of velocity recovery and loss of total pressure. Pressure recovery coefficient (C_p) is defined as the increase in static pressure divided by the velocity energy entering the diffuser. The CFD solution reported a pressure recovery coefficient of 0.60, indicating that 60 percent of the velocity energy was recovered. Pressure loss coefficient (K) is defined as the loss in total pressure through the diffuser divided by the velocity energy entering the diffuser. The CFD solution reported a pressure loss coefficient of 0.28, which indicates that 28 percent of the velocity energy entering the diffuser was lost. The remaining 12 percent of the energy exits the stage as velocity.

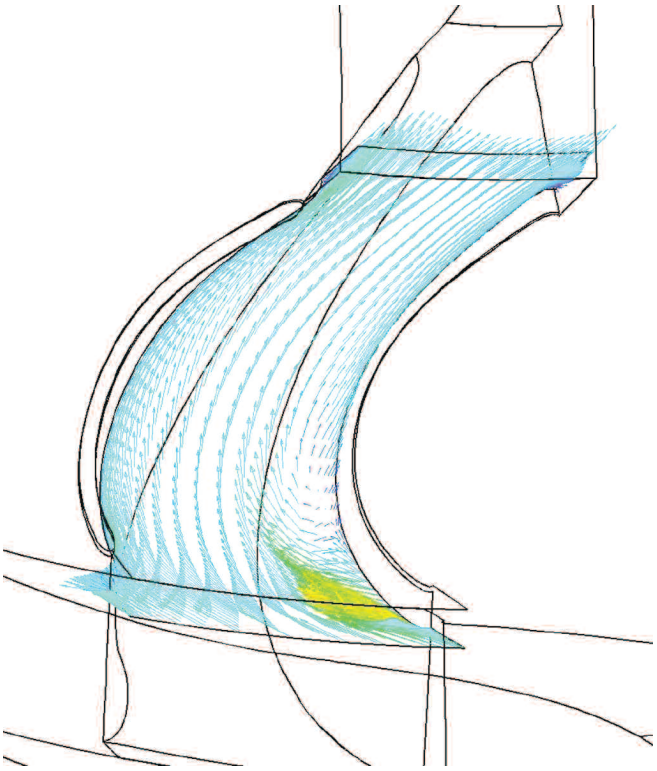

Figure 6. Relative Velocity Vectors near Shroud of Final Design.

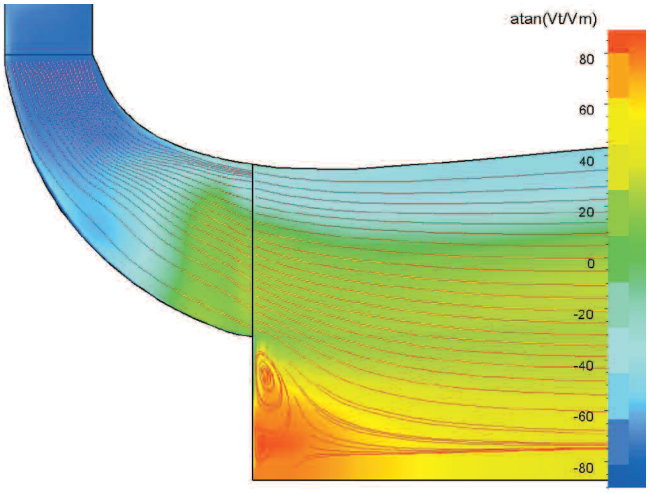

Figure 7. Absolute Flow Angle (Contour) and Streamlines, Discharge from Impeller into Diffuser.

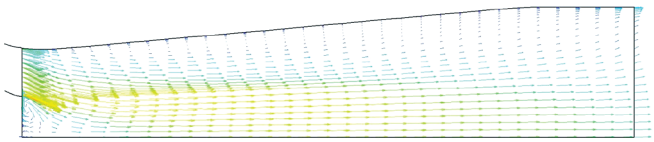

Figure 8. Absolute Velocity Vectors in Expander Conical Diffuser.

Test

The stage was manufactured with the improved impeller design. A successful factory test of the turboexpander stage confirmed CFD results. The machine was subsequently installed and is currently operating successfully in the field.

CASE 2—MIXED-FLOW COMPRESSOR DESIGN

In high-flow, low-pressure ratio compressor applications, "mixed-flow" impellers can be used to minimize the size and cost of the machine. These impellers represent a mixture between an axial impeller and a radial impeller. In the case of a turboexpander-compressor, the "mixed-flow" impeller may allow the unit to run at a speed that gives more optimum operation of the expander. There are few design guidelines available in the literature for very highly mixed-flow compressors, and the designer benefits greatly from the insight provided by CFD.

For this design, a previous test with the same impeller design had shown good stage efficiency of 77 percent. CFD was applied to this design to try to improve the range and to see if the efficiency could also be improved. Testing would eventually determine the net result of any geometric changes, but unless expensive laser measurements were used, detailed information on the flow field would not be available.

The mixed-flow stage was designed using conventional design tools and the 3-D blade design and analysis software. The multi-stream-tube analysis showed uniform diffusion in the impeller and reasonable blade loading, although somewhat high loading at the impeller exit.

Finding no obvious deficiencies in the impeller design, a CFD model was constructed to understand the nature of the flow. The CFD model included an axial inlet section, unshrouded impeller with tip clearance, and the pinched vaneless diffuser. The CFD software's implementation of the Baldwin-Lomax turbulence model was used.

CFD results revealed a complex interaction between the wheel and diffuser, which resulted in a large flow recirculation on the hub side of the diffuser bend and a highly skewed velocity profile throughout the diffuser. The recirculation zone increased in size at lower flowrates, extending upstream to the middle of the impeller at 85 percent flow. The recirculation does not occur at 130 percent flow. This diffuser flowfield is shown in Figures 9 and 10.

The rotor efficiency was 93 percent per CFD, confirming 3-D blade design software conclusions that the rotor blading was reasonable. The velocity and flow angle of the gas can be assessed at various stations through the diffuser, as shown in Figure 11. Figures 12 and 13 show that the skewing of the velocity profile actually worsens as the flow moves through the bend, even with the substantial pinching of the passage height.

Integrating Across Surfaces

The flow through any plane of a CFD solution can be interrogated to quantify the flowfield. Much insight can be gained by considering the "area-averaged meridional velocity" and the "mass-averaged meridional velocity." The area-averaged meridional velocity is obtained by integrating the meridional velocity across the area of a plane normal to the flow. This gives approximately the same value as simply dividing the total volumetric flow by the throughflow area, and represents the "ideal velocity" that would exist if the velocity were uniform.

The mass averaged meridional velocity is obtained by integrating the weighted velocity through the surface, as shown in Equation (4).

$$Vm,\ Mass\ Averaged = \left[\frac{\int_s \vec{V}_{xyz} \bullet dS \bullet (\rho \cdot v_m)}{\int_s \vec{V}_{xyz} \bullet dS \bullet \rho} \right] \qquad (4)$$

where:
V_{xyz} = Local absolute velocity vector
S = Surface of plane normal to the flow
ρ = Local density
v_m = Local meridional velocity

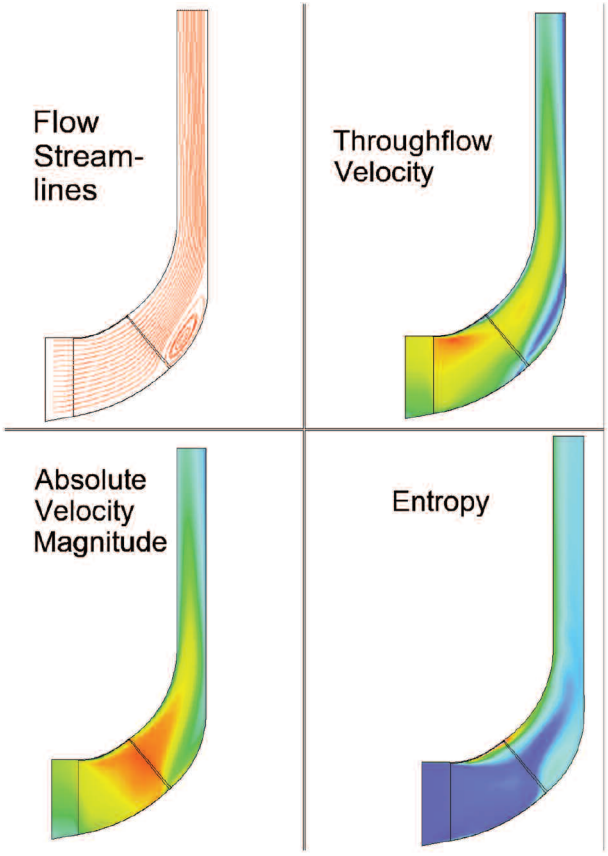

Figure 9. Flowfield in Original Design.

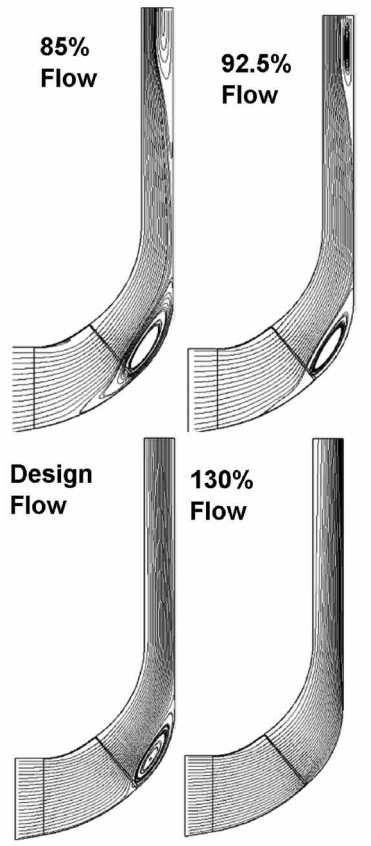

Figure 10. Velocity Streamlines at Various Flowrates for Original Design.

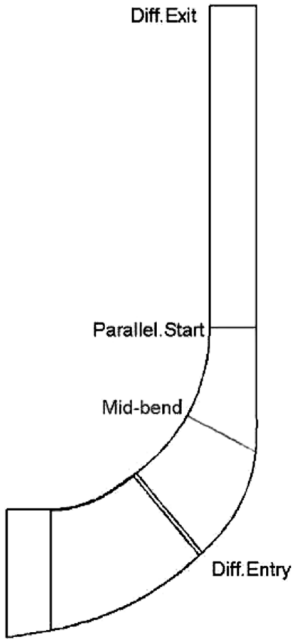

Figure 11. Computational Planes Normal to the Flow for Flow Angle and Velocity Plots.

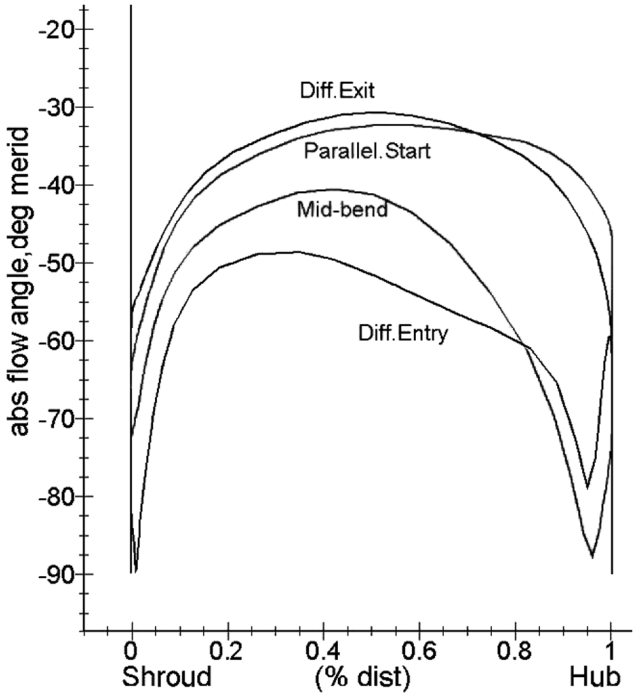

Figure 12. Absolute Flow Angle at Four Locations in the Diffuser (Original Design).

A plot of mass-averaged and area-averaged velocity (Figure 14) clearly illustrates the effect of nonuniform flow in the diffuser. The difference between the mass-average and area-average is due only to blockage from recirculation and the slow-moving boundary layer. This chart shows quantitatively the behavior seen in the velocity streamlines of Figure 10.

The aerodynamic blockage can be defined directly as in Equation (5).

$$Blockage = \frac{v_{m,Mass\ Avg}}{v_{m,Area\ Avg}} - 1 \tag{5}$$

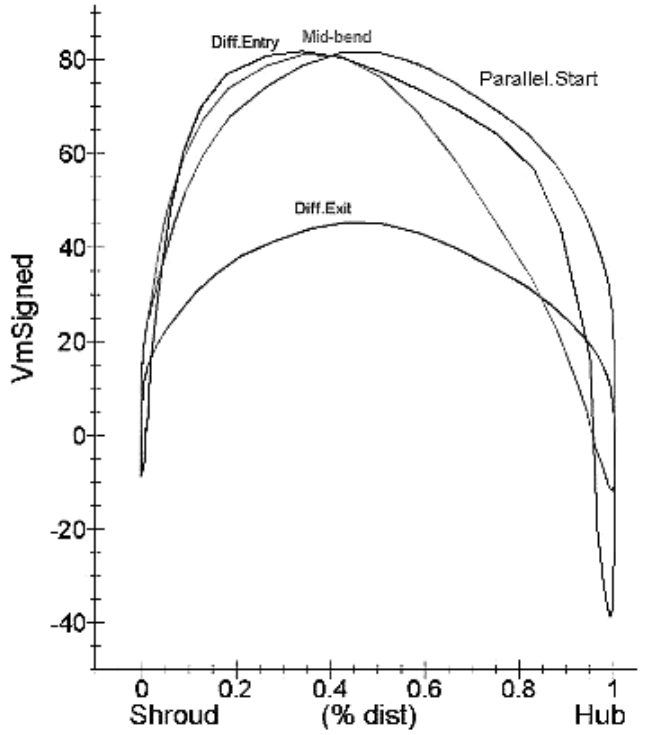

Figure 13. Throughflow Velocity Profile (Vm) at Four Locations in the Diffuser (Original Design).

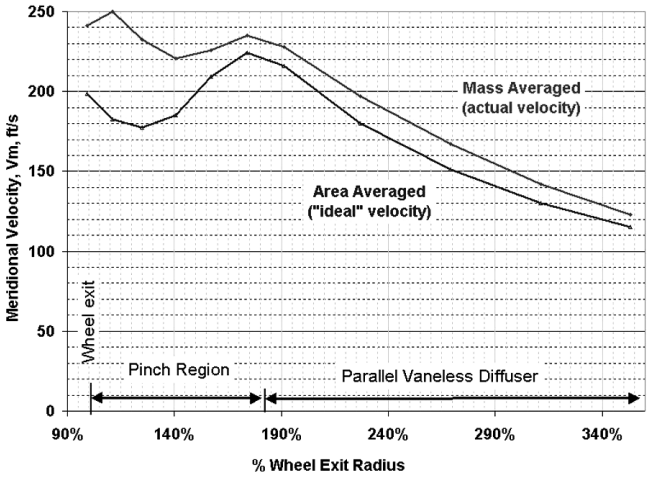

Figure 14. Throughflow Velocity (Meridional), Mass-Averaged and Area-Averaged (Original Design).

This blockage is plotted in Figure 15. This shows clearly that the pinching of the flow needs to occur much more rapidly to prevent recirculation.

Based on this observation, several designs were evaluated in just a few days. These designs attempted to minimize the impeller wake, and also accelerate the flow immediately following the trailing edge of the impeller. The successful design used an aggressive pinch from the hub-side, which 3-D blade design software (Figure 16) predicted to have very low hub-to-shroud loading. This design created the desirable flow field shown in Figure 17 and Figure 18. The velocity profiles and flow angles are plotted in Figures 19 and 20, showing much more uniform velocity and flow angle throughout the bend.

The aerodynamic blockage is plotted in Figure 21. It shows quantitatively the reduction of blockage that was achieved in the final design.

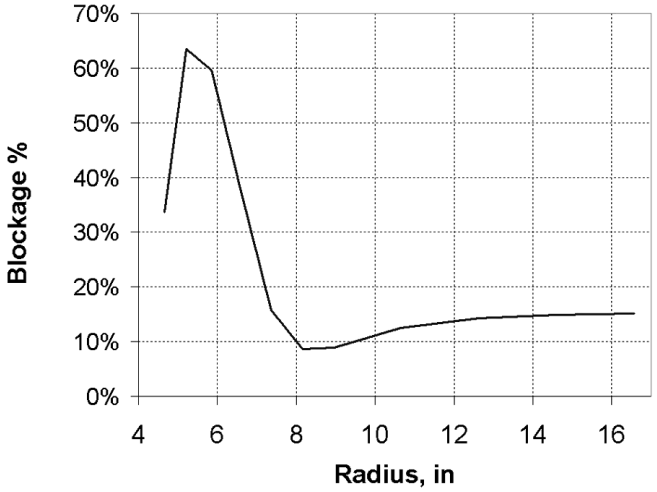

Figure 15. Blockage Plot for Diffuser.

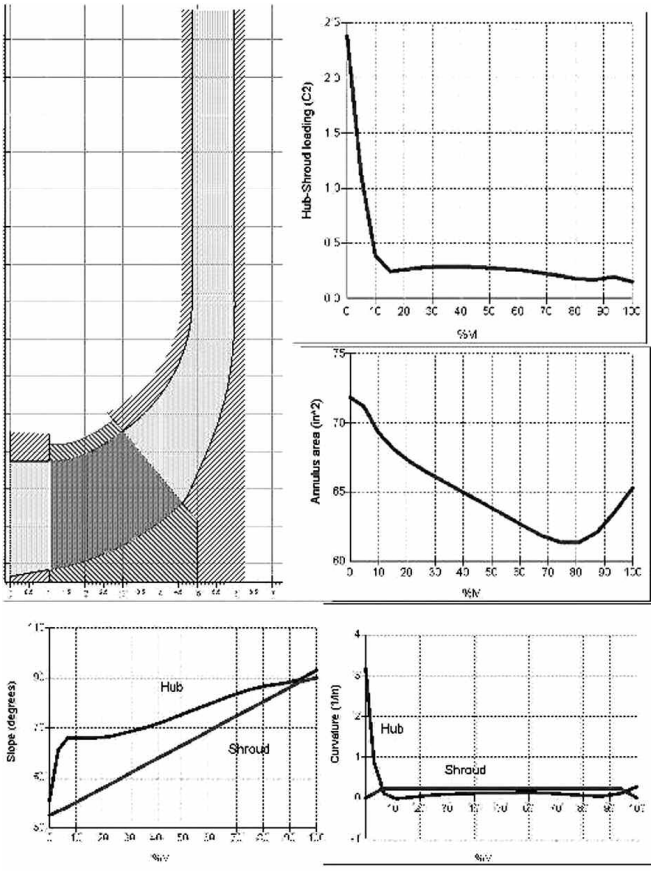

Figure 16. Design of New Diffuser Hub Contour.

Conclusion

The CFD-based diffuser design led to a high performing diffuser, but also reduced the blockage, allowing the diffusion in the impeller to increase significantly. CFD is often used quantitatively to back out the familiar one-dimensional (1-D) parameters, which allows designs to be easily evaluated. For this design, the diffuser recovery (C_p) was increased from .71 to .75, and the total pressure loss in the diffuser (k) was reduced from .15 to .10. The velocity at the wheel exit was reduced from 48 percent of the stage head to 40 percent, and the velocity at the diffuser exit was reduced from 6.4 percent to 5.8 percent. The velocity ratio through the impeller was reduced from .80 to .70, and the polytropic stage

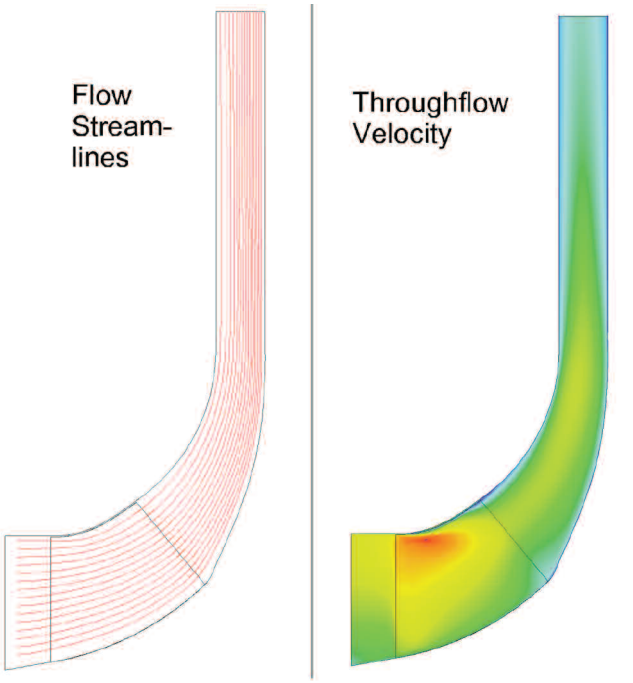

Figure 17. Final Design Contours, Meridional Velocity and Velocity Streamlines.

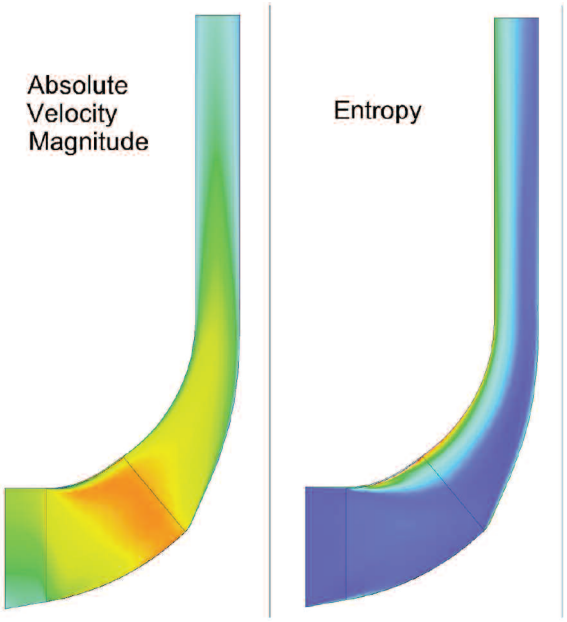

Figure 18. Final Design Contours, Entropy and Magnitude of Absolute Velocity.

efficiency was increased from 79.5 percent to 84 percent, according to CFD. The test result for the stage showed efficiency slightly higher than 84 percent, confirming that very large gains were made with the careful use of CFD.

CASE 3—OIL LUBRICATED THRUST BEARING

Although CFD tools in turbomachinery are most often applied to the aerodynamic flow path, it is also useful in understanding oil lubricated bearings, as in the case of the tapered land thrust bearing shown in Figure 22. One of the many interesting features of a typical turboexpander is the automatic thrust equalizer, or ATE (refer to Figure 23). This device uses actual pressures measured on the thrust faces to actively control the amount of axial force on the

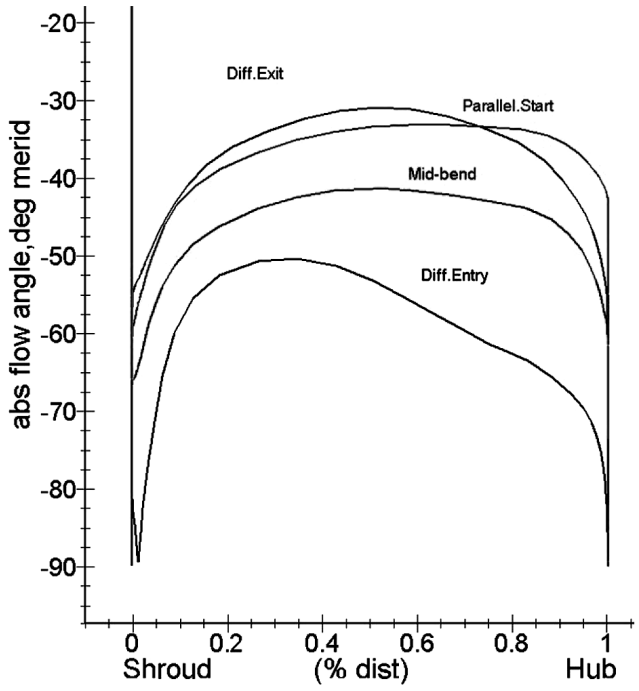

Figure 19. Absolute Flow Angle at Four Locations in Diffuser (Final Design).

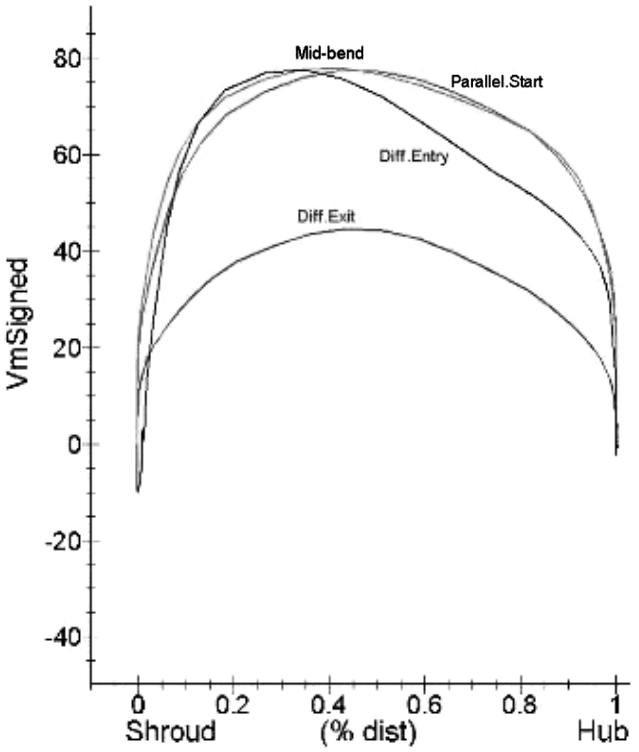

Figure 20. Throughflow Velocity Profile (Vm) at Four Locations in Diffuser (Final Design).

thrust bearings. While reviewing the design details of a particular thrust bearing, it was decided to perform CFD calculations to:

- Compare the results with the bulk flow calculations normally used for design, and
- Gain insight into the details of the oil film, which simply is not possible with bulk flow calculations.

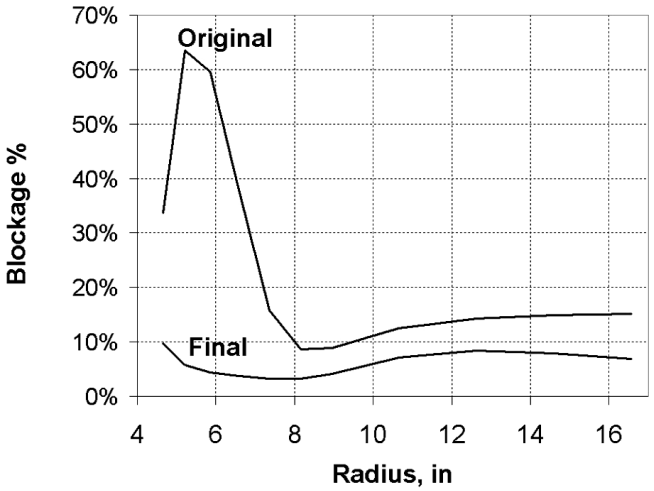

Figure 21. Blockage Plot for Original and Final Diffuser.

Figure 22. Thrust Bearing.

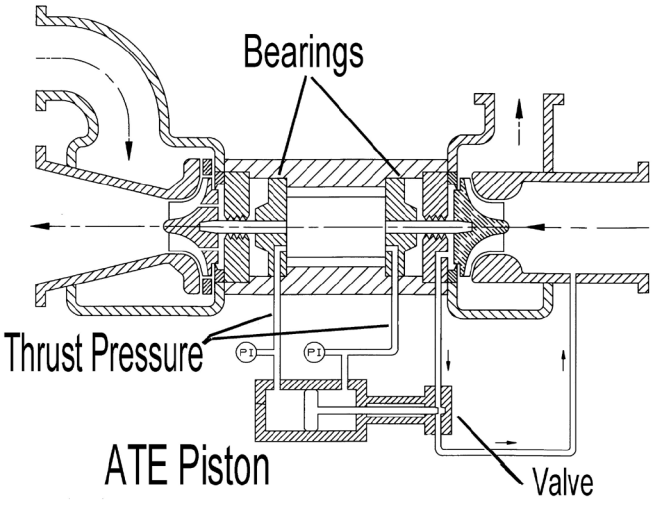

Figure 23. Automatic Thrust Equalizer Schematic (ATE).

Bearing Model

The bearing consists of six tapered land pads, each having its own oil supply orifice. The outer diameter of the thrust runner is 4.6 inches (117 mm). For comparison purposes, all calculations were performed at 22,000 rpm. This results in a peripheral disk velocity of 442 ft/s (135 m/s), which is high relative to many types of rotating machinery, but well within the operating experience of existing turboexpanders.

The CFD analysis was performed for two different oil film thicknesses. The wide gap, 0.006 inches (0.15 mm), corresponds to a predicted axial load of about 100 lbf (445 N). The narrow gap, 0.004 inches (0.10 mm), corresponds to a predicted axial load of about 400 lbf (1780 N). The reason the film thickness values are so large is that the ATE system is designed to control the thrust force to relatively low values, thus the film thickness is normally large. It will be shown later that these values resulted in peak film pressures of approximately 75 psia (5 bara) and 150 psia (10 bara), respectively. It is worth noting at this point that the film pressures discussed here refer to pressures above the bearing's ambient pressure, which is generally not standard atmospheric air pressure, but instead an elevated pressure consisting of process gas contained in the hermetically sealed bearing cavity. For this analysis, the bearing was assumed to be operating in a 65 psia environment.

The model used to represent the bearing was quite detailed. A very fine mesh density was needed to resolve the small clearance into sufficient segments to accurately model the flow. The oil flow into the bearing was not a fixed boundary condition. In real life, the pressure upstream of an oil control orifice is held constant, and the oil flow can vary somewhat as the pressure in the bearing fluctuates. To increase the accuracy of the model, this orifice was included in the CFD model.

Pressure Profile

Figure 24 shows the CFD results for pressure profiles in the oil film at a distance midway between the shaft and the bearing. Other cutting planes were evaluated, but the results were nearly identical. Note that the peak pressure of 74.5 psia is located near the trailing edge and is about 75 percent out from the inner edge of the pad. It is not obvious from this picture, but the leading edge of the pad consists of an oil inlet pocket and thus is not really part of the hydrodynamic surface. This will become more obvious when the temperature plots are examined.

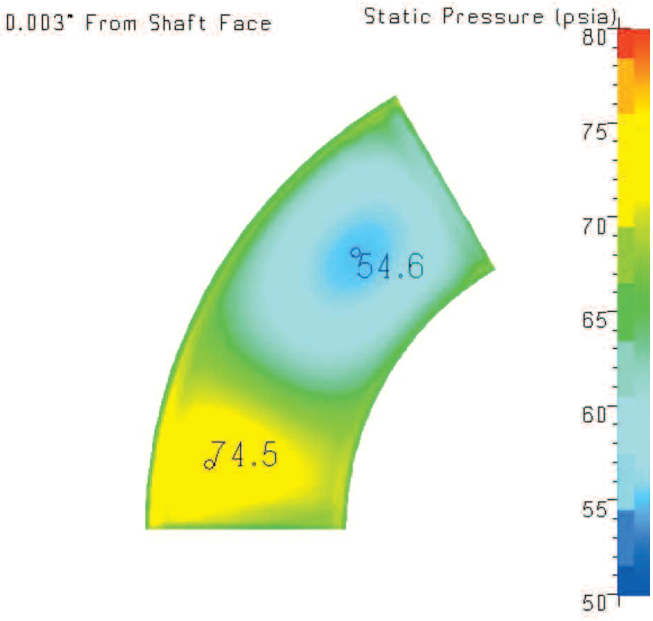

Figure 24. Static Pressure in Oil Film, Large Clearance (.006 Inch).

When the clearance is reduced to 0.004 inch, the expectation is that the film pressure will rise, and this is exactly what is seen in

Figure 25. Again, only the results at the center of the oil film (halfway between the shaft and the bearing) are shown, since all other cutting planes examined were nearly identical. For this case, the peak bearing pressure is calculated to be about 148 psia.

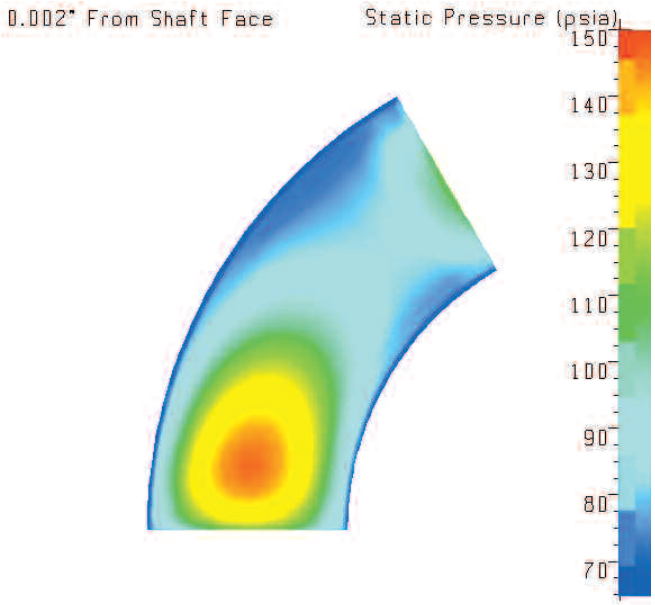

Figure 25. Static Pressure in Oil Film, Small Clearance (.004 Inch).

Temperature Profiles

The temperature of the 0.006 inch (0.15 mm) oil film, with several cutting planes from the shaft face to the bearing face, is shown in Figure 26. The location of the oil feed pocket can be readily seen at the leading edge of the pad in Figure 26e, since the inlet oil is much cooler than the rest of the oil in the oil film.

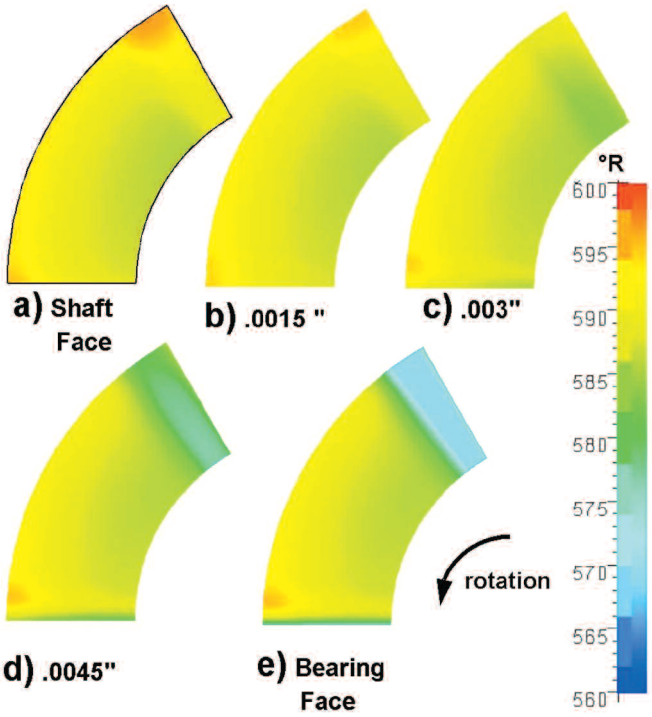

Figure 26. Static Temperature (°R) at Various Distances Between Shaft and Bearing, Large Clearance.

It is interesting to note that the cooling effect of the inlet oil seems to dissipate rapidly in the oil film, so that the location of the oil inlet pocket is barely noticeable in the oil temperatures at the midplane location, Figure 26c. The effect of hot oil carryover, which can be seen at the outer portion of the leading edge of the pad, can be observed in Figure 26a, and will be discussed in more detail later.

The temperature of the oil film when the clearance is reduced to 0.004 inch (0.1 mm) can be seen in Figure 27. The cutting planes again start near the shaft and progress toward the bearing. The results for the tighter clearance are similar to those for the larger clearance. As expected, the regions of warm temperature are noticeably warmer when the bearing clearance is reduced.

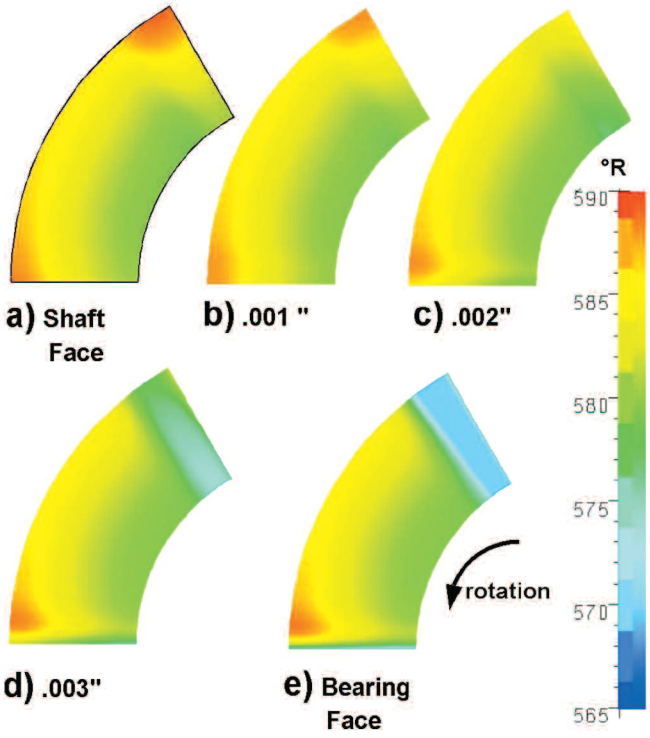

Figure 27. Static Temperature (°R) at Various Distances Between Shaft and Bearing, Small Clearance.

In Figure 27a, the cutting plane nearest the shaft, it can be seen that the oil at the leading edge of the pad in the area of the oil inlet groove is much warmer than the inlet oil (which is the large blue region of Figure 27e). This is due to hot oil carryover from the trailing edge of the preceding pad.

To better understand the hot oil carryover, an imaginary massless particle was released into the oil film to plot the trajectory of the oil through the bearing. This particle was released at the midplane position, near the bore of the bearing. Figure 28 shows the path for 0.006 inch (0.15 mm) clearance, and Figure 29 shows the path for 0.004 inch (0.1 mm) clearance. It can be seen that the larger axial clearance allows a more direct radial path for the oil to escape the bearing, whereas the tighter clearance forces the oil into a more tangential path before exiting the bearing. For the large clearance, a particle dropped at the inlet to the first pad will leave the bearing by the time it gets to the second pad. For the small clearance, a particle dropped at the first pad will remain in the bearing longer, exiting at the fourth pad.

Comparison with Bulk Flow Calculations and Test Data

This investigation included comparisons of the CFD results with a commercial bearing code, two inhouse programs, and actual test data. The results are shown in Figure 30. To obtain the test data, an actual

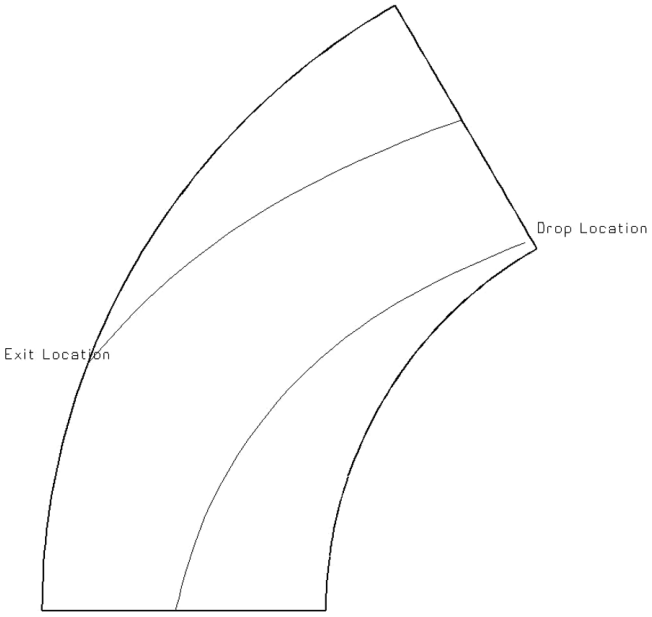

Figure 28. Velocity Streamline for Particle Released into Large Clearance.

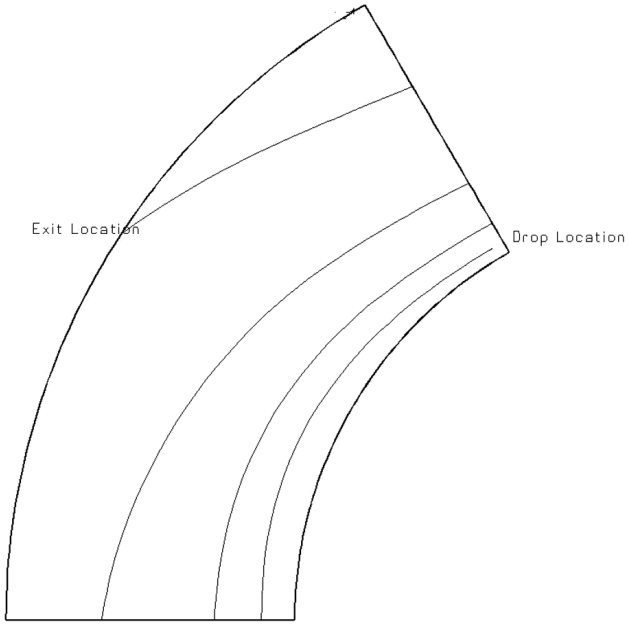

Figure 29. Velocity Streamline for Particle Released into Small Clearance.

production machine was used. A means of axially loading the bearings while running at 22,000 rpm was developed, and bearing clearance information was obtained using specially installed eddy current probes. The results show reasonable agreement in the area of interest (0.004 inch to 0.006 inch, or 0.15 mm to 0.1 mm).

Benefit of CFD

This investigation revealed that the existing bulk flow calculations routinely used for design are acceptable in the areas in which they are normally used. The CFD calculations proved useful mainly as a means of understanding the character of the flow and the distribution of temperature and pressure in the oil film. The results identified the best location for sensing the pressure in the bearing to allow proper positioning of the ATE sensing port and provided better understanding of the nature of the hot oil carryover

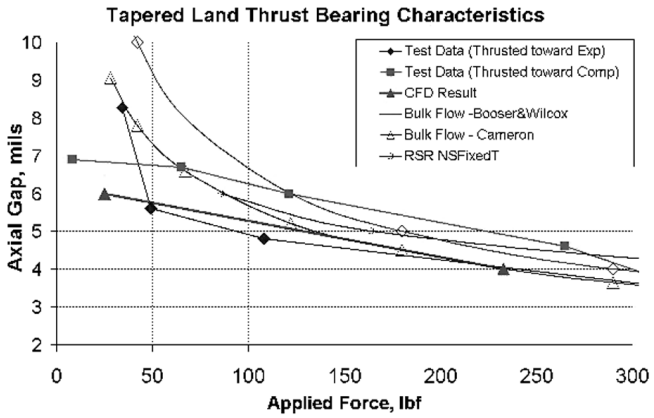

Figure 30. Comparison of Test Data, CFD, and Bulk Flow Calculations.

in the bearing. Thermal distortion of the bearing metal was not included in this model, but current projects are exploring thermal distortion effects on bearing performance.

CASE 4—TROUBLESHOOTING COMPRESSOR PERFORMANCE

The test of a new high Mach number compressor stage configuration revealed that the surge margin was substantially less than expected. CFD was used to "test" the hardware changes before the actual modifications were made, so that the solution could be implemented with confidence.

Model

The original compressor stage configuration is shown in Figure 31. This is an open centrifugal compressor impeller with a vaneless diffuser that turns the flow 45 degrees at the exit of the diffuser. The application required a high head, high Mach number design. The diffuser originally had only a slight "pinch" (tapering of the wall at the inlet to the diffuser). The CFD model incorporated a short inlet section, the compressor impeller with tip clearance, the pinched section, the vaneless diffuser, and the axial turning section.

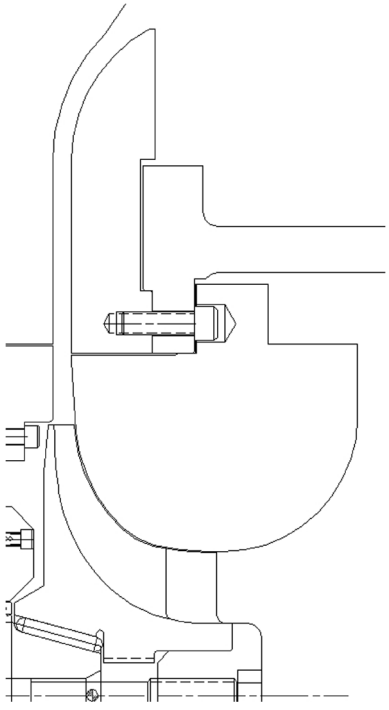

Figure 31. Original Diffuser Geometry.

Problem

When tested, the stage exhibited surge at about 92 percent of design flow. This was higher than expected. Evaluation of the data from the test as well as the design calculations revealed that the most likely cause of the problem was the diffuser.

It was decided to analyze the stage with CFD as it was originally designed as well as with the proposed modifications to the diffuser. The purpose of running the CFD was to ensure that the proposed modifications would solve the problem. The machine was scheduled to ship in a relatively short time frame, and thus it was important to solve the problem in one iteration.

It should be noted that using CFD to predict surge is a difficult task. With the proper choice of modeling equations, boundary conditions, and mesh density, CFD does a good job of predicting passage recirculation. However, surge is a transient flow reversal, which cannot be modeled with a steady-state CFD model. With this in mind, a method will be discussed below that allowed CFD to be used to achieve the desired results.

Method

The first step was to create a model and run it at 92 percent flow, the surge point for the original hardware. This is shown in Figure 32a, and reveals a large recirculation zone along the front (shroud) wall of the diffuser. The level of recirculation shown became the baseline, which represented surge for this stage.

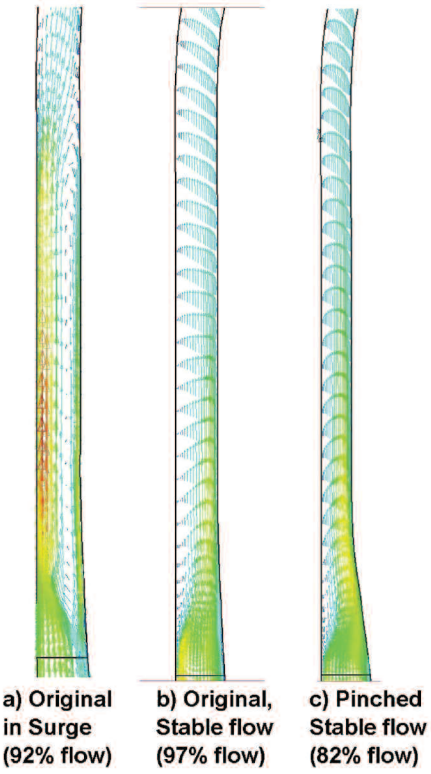

Figure 32. Original Diffuser in Surge (92 Percent), Original Diffuser out of Surge (97 Percent), Pinched Diffuser at Low Flow (82 Percent).

The next step was to run the same model at conditions representing 97 percent of design flow. The results are shown in Figure 32b, and indicate that diffuser recirculation is almost completely gone, and the region of low momentum fluid shifted to the back (hub) wall of the diffuser.

The proposed modification to the diffuser consisted of machining the shroud wall of the diffuser to achieve greater pinch and then moving the entire shroud wall over to decrease the diffuser width. This modification is shown in Figure 33. A third CFD run was then made with the model changed to reflect the proposed hardware changes and run under conditions representing 82 percent of design flow. This flow point was important because the stage would be considered to have an acceptable surge margin if it surged at or below this point. By running the CFD here, we could compare the results with the original configuration at surge and 5 percent above surge and thus determine if the modification would be successful.

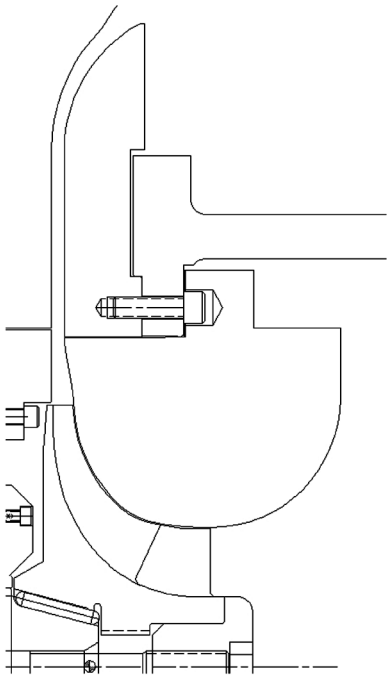

Figure 33. Pinched Diffuser Geometry.

Figure 32c shows that the modified hardware has a region of low momentum fluid near the hub wall that is similar to the results obtained with the original hardware operating at a flow point 5 percent above actual surge. This relatively stable flow meant that surge could be expected to be better than what was required for the stage. In fact, we could reasonably expect that it might be better by at least 5 percent, based on the similarity of Figure 32b and 32c.

A final CFD run was made at a flow rate of 112 percent of design flow, which represented the highest off-design for the stage. The purpose of this run was to make sure that the smaller diffuser gap did not adversely affect the stage performance at the higher flow rates. Figure 34 shows the results of this run, which demonstrated that the flow is reasonably uniform at this flowrate, and the losses in the diffuser did not radically change.

Test Results

Based on the promising CFD results, the proposed hardware modifications were implemented. The machine was returned to the test stand and the new surge margin was measured at 74 percent while the efficiency of the stage remained above the guarantee point. The solution was deemed a complete success. The polytropic head curve is shown in Figure 35.

It is worth noting here that Figure 35 shows the compressor stage performance while running at the appropriate PTC-10 (1997) test speed. Note that high head and high Mach number conspire to limit the range of any centrifugal compressor. If this stage were tested at a speed below the PTC-10 (1997) test speed, the surge would occur at a lower flow, and the choke would occur at a higher flow. These would be erroneous test results! This is mentioned because experience has shown that not all manufacturers test their

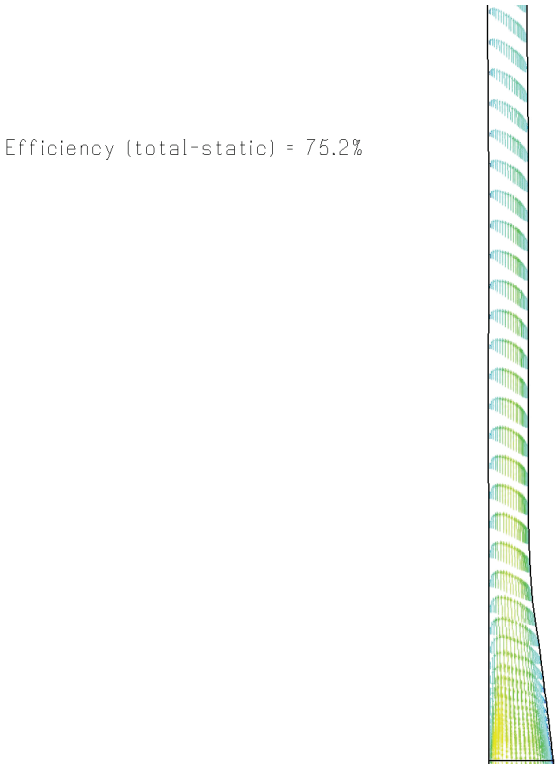

Figure 34. Pinched Diffuser at 112 Percent Flow.

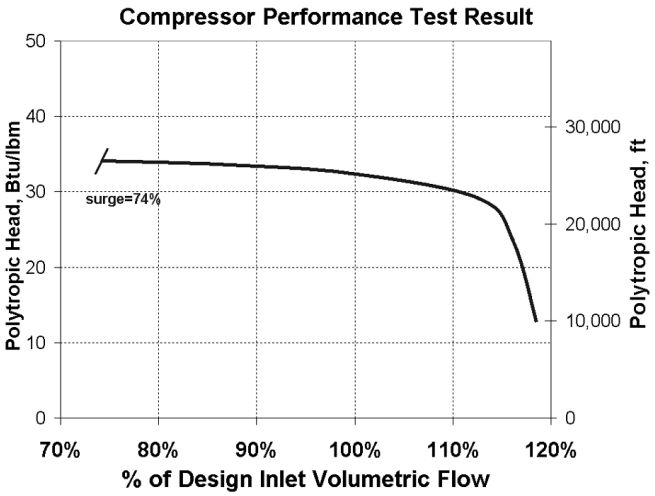

Figure 35. Final Performance Test Result (Pinched Diffuser).

equipment at the appropriate PTC-10 (1997) test speed, and as a result the test curves obtained can look much better than the compressor will actually perform in the field under true process conditions. This can cause many field problems that will be completely avoided if the proper test speed is selected during testing. CFD runs for the choking portion of the curve were not done for this compressor. However, experience with many other stages has shown that CFD is extremely useful in predicting the onset and performance degradation in the choked flow region.

This machine has since been installed in a large ethylene plant in South America (Figure 36) and is running well, with no problems related to surge or choke.

Benefit of CFD

This case provides a clear example of how CFD was used to quickly troubleshoot a problem on the test stand and verify that the proposed solution would work when installed. Although it is a steady-state analysis, the CFD model was "calibrated" to quickly help locate the surge point after hardware modifications.

Figure 36. Final Installation Location.

It is interesting to note that the graphical CFD output was able to be e-mailed to the Chief Engineer, who was on a business trip during part of this process, for review and approval of the proposed changes. Likewise, the customer was able to visually see where the problem was and that the proposed solution was likely to be successful. Perhaps most important, the "tested" solution was first obtained in the virtual world of the computer without any hardware changes or test stand time, after which the actual hardware was modified and successfully tested in a single iteration.

CONCLUSION

In this paper, four case studies were reviewed in which CFD proved to be very helpful to the manufacturer of the equipment. These applications included using CFD to analyze a radial inflow expander stage, two compressor stages, and an oil lubricated tapered land thrust bearing.

The versatility of CFD can readily be seen in the thrust bearing case study, in which five different cutting planes were used to obtain meaningful pressure, temperature, flow, and velocity information in the oil film, all inside a bearing clearance of only 0.004 inches (0.1 mm)!

While some of the work presented here was performed by an individual with a Ph.D. level degree, it should be pointed out that with substantive guidance from CFD experts at the CFD software manufacturer, these tools are very accessible to B.S. level engineers. Recent advances in the software have greatly improved the process of mesh generation and flow visualization. In the past, CFD capability also required a significant capital expenditure for the workstations required to run the code, but modern high-end desktop personal computers (PCs) are capable of running models such as those presented in this paper in just a few hours.

The authors would like to leave the reader with two thoughts concerning CFD use in turbomachinery:

- The manufacturer has determined that direct CFD solutions are very valuable to design and troubleshooting efforts. However, the authors have observed what they call "CFD influenced" design and troubleshooting. This means that the insight gained from any given CFD analysis is proving to be very useful in expanding the understanding of all similar equipment, even if CFD is not specifically used on this other equipment. A similar effect was observed many years ago, when finite element analysis (FEA) was first being used for stress and modal analysis. After the first few FEA results were reviewed for a given basic pressure containing housing, the areas of particular concern were observed to be in similar locations; thus, even without FEA, design and troubleshooting efforts were

enhanced based on this knowledge. Similar effects are now happening with CFD.

- CFD is a "tool," more than a "solution." CFD can tell you what you have, not how to make it better. That is where the experienced engineer comes in. In the future, as more forms of artificial intelligence are developed for use in CFD and FEA software, practical optimization and troubleshooting routines will be used. But the practical constraints of time, cost, safety, materials, etc., make the overall problem unique in almost every instance, ensuring engineers a place in the process for the foreseeable future!

REFERENCES

API Standard 617, 2002, "Axial and Centrifugal Compressors and Expander-Compressors for Petroleum, Chemical and Gas Industry Services," Seventh Edition, American Petroleum Institute, Washington, D.C.

ASME PTC-10, 1997, "Performance Test Code on Compressors and Exhausters," American Society of Mechanical Engineers, New York, New York.